# Structural and Functional Studies of QdtC: An *N*-Acetyltransferase Required for the Biosynthesis of dTDP-3-Acetamido-3,6-dideoxy-α-D-glucose[†,‡]

James B. Thoden,[§] Paul D. Cook,[§] Christina Schäffer,[||] Paul Messner,[||] and Hazel M. Holden*[,§]

*Department of Biochemistry, University of Wisconsin, Madison, Wisconsin 53706, and Department für NanoBiotechnologie, Universität für Bodenkultur Wien, A-1180 Wien, Austria*

*Received December 18, 2008; Revised Manuscript Received February 2, 2009*

ABSTRACT: 3-Acetamido-3,6-dideoxy-α-D-glucose or Qui*p*3NAc is an unusual dideoxy sugar found in the O-antigens of various Gram-negative bacteria and in the S-layer glycoprotein glycans of some Gram-positive bacteria. It is produced in these organisms as a dTDP-linked sugar, with five enzymes ultimately required for its biosynthesis. The focus of this investigation is on the enzyme QdtC, a CoA-dependent *N*-acetyltransferase that catalyzes the last step in the Qui*p*3NAc biosynthetic pathway. For this analysis, three crystal structures were determined: the wild-type enzyme in the presence of acetyl-CoA and two ternary complexes of the enzyme with CoA and either dTDP-D-Qui*p*3N or dTDP-3-amino-3,6-didexoy-α-D-galactose (dTDP-D-Fuc*p*3N). Each subunit of the trimeric enzyme is dominated by a left-handed β-helix motif with 11 turns. The three active sites are located at the subunit−subunit interfaces, and the two dTDP-sugar ligands employed in this study bind to the protein in nearly identical manners. Those residues responsible for anchoring the hexose moieties of the dTDP-sugars to the protein include Glu 141, Asn 159, and Asp 160 from one subunit and His 134 from another subunit. To probe the roles of various amino acid residues in the catalytic mechanism of the enzyme, 10 site-directed mutant proteins were constructed and their kinetic parameters measured. On the basis of these data, a catalytic mechanism is proposed for QdtC in which the acetylation of the sugar amino group does not require a catalytic base provided by the protein. Rather, the sulfur of CoA functions as the ultimate proton acceptor.

Unusual deoxysugars are found throughout Nature, often in the lipopolysaccharides of Gram-negative bacteria (*1*) and on various antibiotics (*1, 2*), antifungals (*3*), anthelmintics (*4*), and antitumor drugs (*5*). One such sugar derivative, 3-acetamido-3,6-dideoxy-α-D-glucose or Qui*p*3NAc,[1] has been observed in the O-antigens of various Gram-negative bacteria, including *Escherichia coli* O114 (*6*), and in the S-layer glycoprotein glycans of some Gram-positive bacteria (*7*). Nucleotide-activated sugar precursors such as dTDP-D-Qui*p*3NAc serve as the building blocks for the formation of either the S-layer glycans or the O-antigens.

In *Thermoanaerobacterium thermosaccharolyticum* E207-71, a Gram-positive, anaerobic, thermophilic organism, five enzymes are required for the biosynthesis of dTDP-D-Qui*p*3NAc starting from glucose 1-phosphate (Scheme 1). Like most of the pathways for the synthesis of 3,6-dideoxyhexoses, the formation of this unusual sugar begins with the attachment of α-D-glucose 1-phosphate to a nucleotide via the action of glucose-1-phosphate thymidylyltransferase (RmlA). In the next step, the 6′-hydroxyl group is removed and the C-4′-hydroxyl group is oxidized to a keto functionality, yielding dTDP-4-keto-6-deoxyglucose. This reaction is catalyzed by dTDP-glucose 4,6-dehydratase (RmlB). Both the thymidylyltransferase and the dehydratase have been well characterized with respect to structure and function (*8*).

Three additional enzymes are ultimately required for the synthesis of dTDP-D-Qui*p*3NAc: an isomerase, an aminotransferase, and an *N*-acetyltransferase (Scheme 1). The focus of this investigation is on the *N*-acetyltransferase, which is encoded by the *qdtC* gene and hereafter termed QdtC (*9*). The protein contains 265 amino acid residues, requires acetyl-CoA for activity, and, interestingly, can acetylate either dTDP-D-Qui*p*3N or dTDP-3-amino-3,6-dideoxy-α-D-galactose (dTDP-D-Fuc*p*3N). Here we present a combined structural and functional analysis of QdtC. For this investigation, three structures of QdtC were determined: one with bound acetyl-CoA and two as ternary complexes with CoA and either dTDP-D-Qui*p*3N or dTDP-D-Fuc*p*3N. On the basis of these structures, site-directed mutant proteins were subsequently constructed to probe the biochemical roles for five residues in the catalytic mechanism, namely, His 123, His

[†] This research was supported in part by NIH Grant DK47814 to H.M.H.

[‡] X-ray coordinates have been deposited in the Protein Data Bank (PDB), Research Collaboratory for Structural Bioinformatics, Rutgers University, New Brunswick, NJ, as entries 3FSA, 3FSB, and 3FSC.

* To whom correspondence should be addressed. E-mail: Hazel_Holden@biochem.wisc.edu. Fax: (608) 262-1319. Phone: (608) 262-4988.

[§] University of Wisconsin.

[||] Universität für Bodenkultur Wien.

[1] Abbreviations: CoA, coenzyme A; Fuc*p*3N, 3-amino-3,6-dideoxy-α-D-galactose; Fuc*p*3NAc, 3-acetamido-3,6-dideoxy-α-D-galactose; HEPES, 4-(2-hydroxyethyl)-1-piperazineethanesulfonic acid; HEPPS, 3-[4-(2-hydroxyethyl)-1-piperazine]propanesulfonic acid; IPTG, isopropyl β-D-thiogalactopyranoside; NiNTA, nickel nitrilotriacetic acid; PCR, polymerase chain reaction; Qui*p*3N, 3-amino-3,6-dideoxy-α-D-glucose; Qui*p*3NAc, 3-acetamido-3,6-dideoxy-α-D-glucose; TB, terrific broth; dTDP, thymidine diphosphate; dTMP, thymidine monophosphate; Tris, tris(hydroxymethyl)aminomethane.

10.1021/bi802313n CCC: $40.75 
Published on Web 02/04/2009

Scheme 1

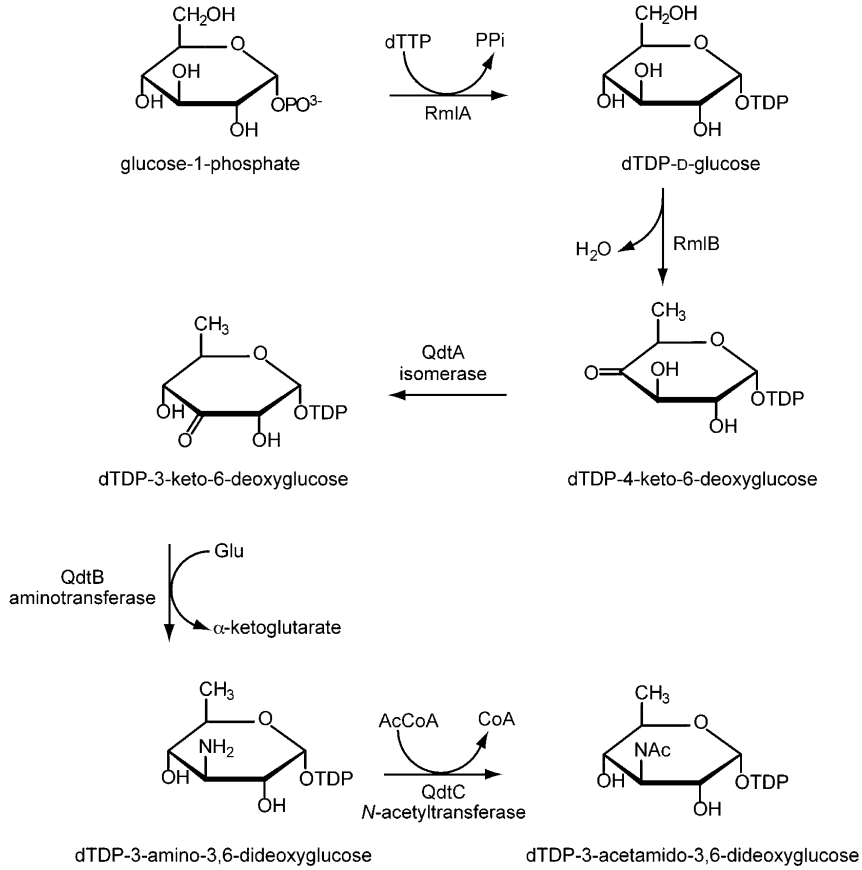


134, Glu 141, Asn 159, and Asp 160. Taken together, the results presented here reveal the overall trimeric structure of QdtC and allow for a novel catalytic mechanism to be proposed.

## MATERIALS AND METHODS

*Cloning, Expression, and Purification.* Genomic DNA from *T. thermosaccharolyticum* E207-71 was isolated by standard procedures. The *qdtC* gene was PCR-amplified from genomic DNA such that the forward primer 5′-AAAA-*CATATG*CCAAATAATATTTCTAAAAGTGC-GATAATAAAAGAAGG and the reverse primer 5′-AAAA*CTCGAG*GTTTTCTATTGAAATATTCTTTATCCA TGTATCATAATCTGTTTC added NdeI and XhoI cloning sites, respectively. The purified PCR product was A-tailed and ligated into a pGEM-T (Promega) vector for screening and sequencing. A QdtC-pGEM-T vector construct of the correct sequence was then appropriately digested and ligated into a pET31b(+) (Novagen) plasmid for protein production with a noncleavable C-terminal $His_6$ tag.

The QdtC-pET31 plasmid was used to transform Rosetta(DE3) *E. coli* cells (Novagen). The culture in TB medium was grown at 19 °C with shaking for 24 h and subsequently induced with 0.05 mM IPTG. The cells were allowed to express protein at 19 °C for 24 h after induction. QdtC was purified by standard procedures using NiNTA resin. Following purification, the protein was dialyzed against 10 mM Tris-HCl and 200 mM NaCl (pH 8.0) and then concentrated to 17 mg/mL.

All point mutations of the QdtC-pET31 plasmid construct were created via the Stratagene QuikChange method and sequenced to verify that no other changes had been introduced into the gene. The 10 mutant proteins, as listed, were expressed and purified in the same manner as that for the wild-type enzyme: H123N, H123A, H134N, H134A, E141Q, E141A, N159D, N159A, D160N, and D160A.

*Production of dTDP-D-Quip3N and dTDP-D-Fucp3N.* dTDP-D-Qui*p*3N was synthesized from dTDP-glucose as the initiating ligand. A typical 10 mL reaction mixture contained the following: 20 mM HEPPS (pH 8.5), 5 mM $MgCl_2$, 60 mg of dTDP-glucose, 200 mg of glutamate, 4 mg of dTDP-glucose-4,6-dehydratase, 3 mg of QdtA, and 15 mg of QdtB (Scheme 1). The reaction was allowed to proceed at 37 °C for 7 h. All enzymes were removed via filtration with a 10 kDa cutoff centriprep concentrator, and the enzyme-free reaction products were diluted by 1:4 with water. Purification was achieved by chromatography using a 6 mL Resource-Q column and a 120 mL gradient from 0 to 250 mM ammonium bicarbonate at pH 8.5. The desired product peak was identified by mass spectrometry ($M - H^+$, 546.3 amu). Fractions containing the amino sugar product were pooled and lyophilized until all traces of the buffer had been removed. dTDP-D-Fuc*p*3N was produced in an analogous manner, with the exception that enzymes FdtA and FdtB from *Aneurinibacillus thermoaerophilus* DSM10155 were used (*10*). Typical yields of these two compounds were ~50% based on the starting amount of dTDP-glucose.

*Production of dTDP-D-Quip3NAc.* After the QdtA/QdtB reaction outlined above had been allowed to proceed at 37 °C for 7 h, 5 mg of QdtC and 0.1 mmol of acetyl-CoA were added, and this reaction was allowed to proceed until all of the amino sugar was acetylated (~2 h). The enzymes were

Table 1: X-ray Data Collection Statistics[a]

| | enzyme complexed with acetyl-CoA | gold heavy atom derivative | enzyme complexed with CoA and dTDP-D-Qui*p*3N | enzyme complexed with CoA and dTDP-D-Fuc*p*3N |
|---|---|---|---|---|
| resolution limits (Å) | 30.0−1.7 (1.8−1.7) | 30−2.1 (2.2−2.1) | 30.0−1.95 (2.05−1.95) | 30.0−1.8 (1.9−1.8) |
| no. of independent reflections | 59238 (8384) | 32382 (3822) | 39913 (4815) | 50462 (6644) |
| completeness (%) | 93.9 (81.4) | 97.7 (89.7) | 95.1 (79.9) | 95.9 (82.6) |
| redundancy | 4.5 (1.3) | 4.0 (1.8) | 3.4 (1.4) | 3.8 (1.5) |
| average *I*/average $\sigma(I)$ | 13.0 (2.6) | 13.1 (3.8) | 8.7 (2.3) | 10.7 (2.7) |
| $R_{sym}$ (%)[b] | 6.4 (30.5) | 6.4 (16.7) | 8.4 (26.4) | 7.2 (27.3) |

[a] Statistics for the highest-resolution bin are given in parentheses. [b] $R_{sym} = (|\sum I - \bar{I}|/\sum I) \times 100$.

Table 2: Least-Squares Refinement Statistics

| | enzyme complexed with acetyl-CoA | enzyme complexed with CoA and dTDP-D-Qui*p*3N | enzyme complexed with CoA and dTDP-D-Fuc*p*3N |
|---|---|---|---|
| resolution limits (Å) | 30.0−1.7 | 30.0−1.95 | 30.0−1.8 |
| *R*-factor[a] (overall) (%)/no. of reflections | 17.8/59147 | 18.5/39903 | 16.5/50377 |
| *R*-factor (working) (%)/no. of reflections | 17.4/53219 | 18.3/35917 | 16.2/45405 |
| *R*-factor (free) (%)/no. of reflections | 24.1/5928 | 24.7/3986 | 23.1/4972 |
| no. of protein atoms | 4100[b] | 4116[c] | 4104 |
| no. of heteroatoms | 618[d] | 395[e] | 585[f] |
| average *B* values (Å$^2$) | | | |
| protein atoms | 19.4 | 23.5 | 17.8 |
| ligands | 33.6 | 37.7 | 20.5 |
| solvent | 34.3 | 31.2 | 30.0 |
| weighted rms deviations from ideality | | | |
| bond lengths (Å) | 0.013 | 0.012 | 0.013 |
| bond angles (deg) | 2.1 | 2.1 | 2.3 |
| trigonal planes (Å) | 0.007 | 0.006 | 0.008 |
| general planes (Å) | 0.015 | 0.011 | 0.013 |
| torsional angles[g] (deg) | 17.6 | 18.3 | 17.6 |

[a] *R*-factor $= (\sum|F_o - F_c|/\sum|F_o|) \times 100$, where $F_o$ is the observed structure factor amplitude and $F_c$ is the calculated structure factor amplitude. [b] These include multiple conformations for Asn 20 in subunit 2 of the asymmetric unit. [c] These include multiple conformations for His 90 in subunit 1 and Lys 108 in subunit 2. [d] Heteroatoms include two acetyl-CoA molecules and 498 waters. [e] Heteroatoms include two CoA molecules, two dTDP-D-Qui*p*3N ligands, and 229 waters. [f] Heteroatoms include two CoA molecules, two dTDP-D-Fuc*p*3N ligands, and 419 waters. [g] The torsional angles were not restrained during the refinement.

removed by filtration; the material was diluted with water, and the dTDP-D-Qui*p*3NAc was purified using a 6 mL Resource-Q column and a 120 mL gradient from 0 to 100 mM ammonium bicarbonate at pH 8.5. The peak containing the acetylated product was identified by mass spectrometry ($M - H^+$, 588.4 amu). Fractions containing the acetylated sugar were pooled and lyophilized until all traces of the buffer had been removed. Reactions using purified dTDP-D-Qui*p*3N as the initiating ligand gave a 100% yield of the acetylated sugar when treated with acetyl-CoA and QdtC.

*Structural Analysis of QdtC.* Crystallization conditions were initially surveyed with either the apoprotein or protein incubated with 10 mM acetyl-CoA and 10 mM dTDP by the hanging drop method of vapor diffusion and using a sparse matrix screen developed in the laboratory. Diffraction quality crystals were subsequently grown via the hanging drop method by mixing in a 1:1 ratio the protein incubated with acetyl-CoA and dTDP and 22−26% monomethylether poly(ethylene glycol) 5000 and 2% ethylene glycol at pH 7.0. These crystals belonged to space group *P*3 and contained two monomers per asymmetric unit with the following unit cell dimensions: $a = b = 67.3$ Å, and $c = 112.4$ Å.

X-ray data were measured at 100 K using a Bruker AXS Platinum 135 CCD detector controlled with the Proteum software suite (Bruker AXS Inc.). The X-ray source was Cu Kα radiation from a Rigaku RU200 X-ray generator equipped with Montel optics and operated at 50 kV and 90 mA. These X-ray data were processed with SAINT version 7.06A (Bruker AXS Inc.) and internally scaled with SADABS version 2005/1 (Bruker AXS Inc.). Prior to X-ray data collection, the crystals were transferred to a stabilization solution containing 30% monomethylether poly(ethylene glycol) 5000, 400 mM NaCl, 10 mM dTDP, 10 mM acetyl-CoA, and 15% ethylene glycol. Relevant X-ray data collection statistics are presented in Table 1. For the complexes with the dTDP-amino sugars, the respective nucleotide-linked sugar at 40 mM was substituted for dTDP in the stabilization solutions.

An initial structure was solved with one heavy atom derivative using 10 mM potassium gold(I) cyanide and a soak time of 3 days. Two gold binding sites were identified with SOLVE (*11*), giving an overall figure of merit of 0.41 to 2.1 Å resolution. Solvent flattening with RESOLVE (*12, 13*) generated an interpretable electron density map, which allowed a preliminary model to be constructed using COOT (*14*). There was no interpretable electron density corresponding to dTDP even though the crystals were grown in its presence. Consequently, the structure represents the QdtC−acetyl-CoA binary complex. Coordinates for the complex were refined by TNT (*15*) to an $R_{working}$ of 17.8% for all measured X-ray data from 30 to 1.7 Å resolution. A Ramachandran plot analysis shows that 85.6, 13.6, and 0.9% of the amino acid residues lie within the core, allowed, and generously allowed regions, respectively. Relevant refinement statistics are given in Table 2. This structure served as the search model for the subsequent structural analyses of the enzyme−acetyl-CoA−dTDP-linked sugar ternary complexes via molecular replacement with PHASER (*16*).

As discussed in Results and Discussion, there were no interpretable electron densities for the CoA acetyl groups in

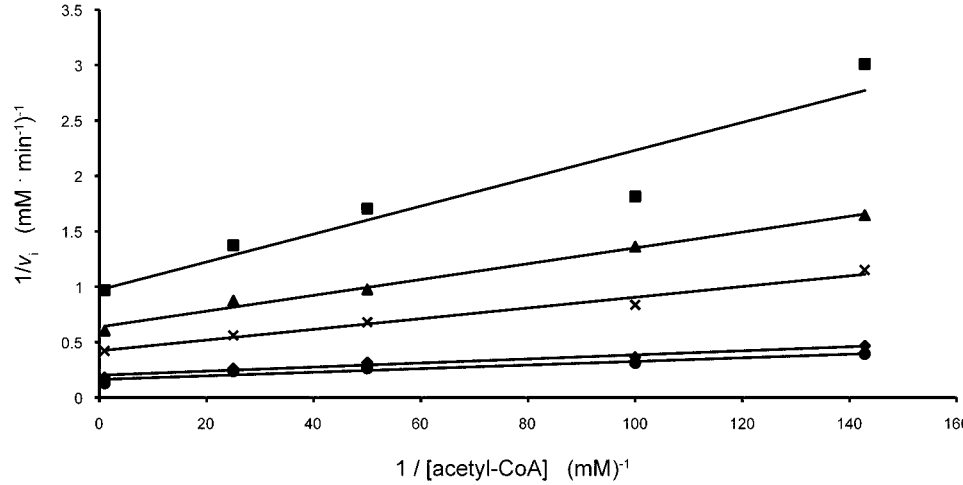


FIGURE 1: Double-reciprocal plots of the initial rates of formation of CoA. In this plot, the concentration of acetyl-CoA is varied at several fixed concentrations of dTDP-D-Qui*p*3N: 0.01 (■), 0.02 (▲), 0.05 (×), 0.2 (◆), and 1.0 mM (●).

Table 3: Kinetic Parameters for the Forward Reaction with dTDP-D-Qui*p*3N and Acetyl-CoA

| protein | $K_m$ (mM) for dTDP-D-Qui*p*3N | $k_{cat}$ ($s^{-1}$) | $k_{cat}/K_m$ ($M^{-1}$ $s^{-1}$) |
|---|---|---|---|
| wild-type | 0.11 ± 0.02 | 8.7 ± 0.4 | $7.9 \times 10^4$ |
| wild-type using dTDP-D-Fuc*p*3N | 0.36 ± 0.06 | 15.2 ± 0.7 | $4.2 \times 10^4$ |
| H134N | 0.60 ± 0.05 | 9.1 ± 0.3 | $1.5 \times 10^3$ |
| H134A | 4.50 ± 0.45 | 10.0 ± 1.0 | $2.2 \times 10^3$ |
| E141Q | 0.72 ± 0.09 | 5.8 ± 0.3 | $8.1 \times 10^3$ |
| E141A | 1.05 ± 0.08 | 44.1 ± 1.0 | $4.2 \times 10^4$ |
| H123N | 0.59 ± 0.08 | 12.3 ± 0.7 | $2.1 \times 10^4$ |
| H123A | 0.63 ± 0.04 | 12.3 ± 0.4 | $2.0 \times 10^4$ |
| D160N | 9.78 ± 0.67 | 12.2 ± 0.3 | $1.2 \times 10^4$ |
| D160A | 10.7 ± 0.8 | 0.25 ± 0.01 | 2.3 × 10 |
| N159D | 0.51 ± 0.08 | 20.3 ± 0.7 | $4.0 \times 10^4$ |
| N159A | 15.4 ± 1.5 | 18.9 ± 1.4 | $1.2 \times 10^3$ |

either of the complexes. Hence, the reported structures represent ternary complexes with the dTDP-linked sugars and CoA rather than acetyl-CoA. Least-squares refinement with TNT reduced the *R*-factor to 18.5% for all measured X-ray data from 30 to 1.95 Å resolution for the protein−CoA−dTDP-D-Qui*p*3N complex and 16.5% for all measured X-ray data from 30 to 1.8 Å resolution for the protein−CoA−dTDP-D-Fuc*p*3N complex. A Ramachandran plot analysis demonstrates that for the enzyme−CoA−dTDP-D-Qui*p*3N complex, 85.0, 14.2, and 0.9% of the amino acid residues lie within the core, allowed, and generously allowed regions, respectively. Likewise, the enzyme−CoA−dTDP-D-Fuc*p*3N complex refined equally as well with 84.7, 14.7, and 0.7% of the amino acid residues located within the core, allowed, and generously allowed regions of the Ramachandran plot, respectively. Relevant refinement statistics are presented in Table 2.

*Measurement of Enzymatic Activity.* *N*-Acetyltransferase activity was monitored spectrophotometrically by following the increase in absorbance at 412 nm due to the reaction of the sulfhydryl group of the CoASH product with 5,5′-dithiobis(2-nitrobenzoic acid) resulting in a disulfide interchange. This interchange leads to the formation of 5-thio-2-nitrobenzoic acid, which has a characteristic absorbance at 412 nm and an extinction coefficient of 14150 $M^{-1}$ $cm^{-1}$. The use of this compound for quantification of CoASH was first reported by Tomkins et al. (*17*), and our assay method was similar to that described in ref *18*. Reactions were monitored continuously with a Beckman DU 640B spectrophotometer, and enzyme activities were calculated from the initial rates. Assay reaction mixtures were 100 μL in volume and contained, in addition to enzyme and substrates, 100 mM HEPES (pH 7.5) and 5 mM 5,5′-dithiobis(2-nitrobenzoic acid). The reactions were initiated by the addition of enzyme and monitored at 25 °C. Kinetic data were fitted using Sigma Plot 8. Initial velocity patterns were evaluated by measuring the initial rates at five concentrations of each substrate, 0.01, 0.02, 0.05, 0.2, and 1.0 mM dTDP-Qui*p*3N and 0.007, 0.01, 0.02, 0.04, and 1.0 mM acetyl-CoA. Equation 1 was used to fit the data, and the double-reciprocal plots clearly showed a series of intersecting lines (Figure 1), suggesting a sequential mechanism.

$$v = VAB/(K_aB + K_bA + K_{ia}K_b + AB) \quad (1)$$

Calculated $K_m$ values were 0.018 ± 0.002 mM for acetyl-CoA and 0.11 ± 0.02 mM for dTDP-Qui*p*3N.

Kinetic constants for the alternate substrate (dTDP-Fuc*p*3N) and the mutant proteins were determined at a saturating concentration of acetyl-CoA, 1.0 mM, while the dTDP-sugar concentrations were varied between 0.01 and 54 mM. Individual substrate saturation kinetic data were fitted to eq 2.

$$v = VA/(K_a + A) \quad (2)$$

The kinetics data are presented in Table 3.

## RESULTS AND DISCUSSION

*Structure of QdtC Complexed with Acetyl-CoA.* The crystals employed in this investigation contained two subunits of QdtC, each of which packed along crystallographic 3-fold rotational axes to generate the physiological trimers. The two subunits in the asymmetric unit are nearly identical and superimpose with a root-mean-square deviation of 0.15 Å. A ribbon representation of the QdtC trimer is displayed in Figure 2a. It is rather elongated with overall dimensions of ∼73 Å × 76 Å × 64 Å. A total of ∼4000 $Å^2$ of surface area per subunit is buried upon trimerization. Each subunit participates in extensive interactions with the other two subunits forming the trimer. The individual acetyl-CoA binding sites, separated by ∼24 Å as measured from the

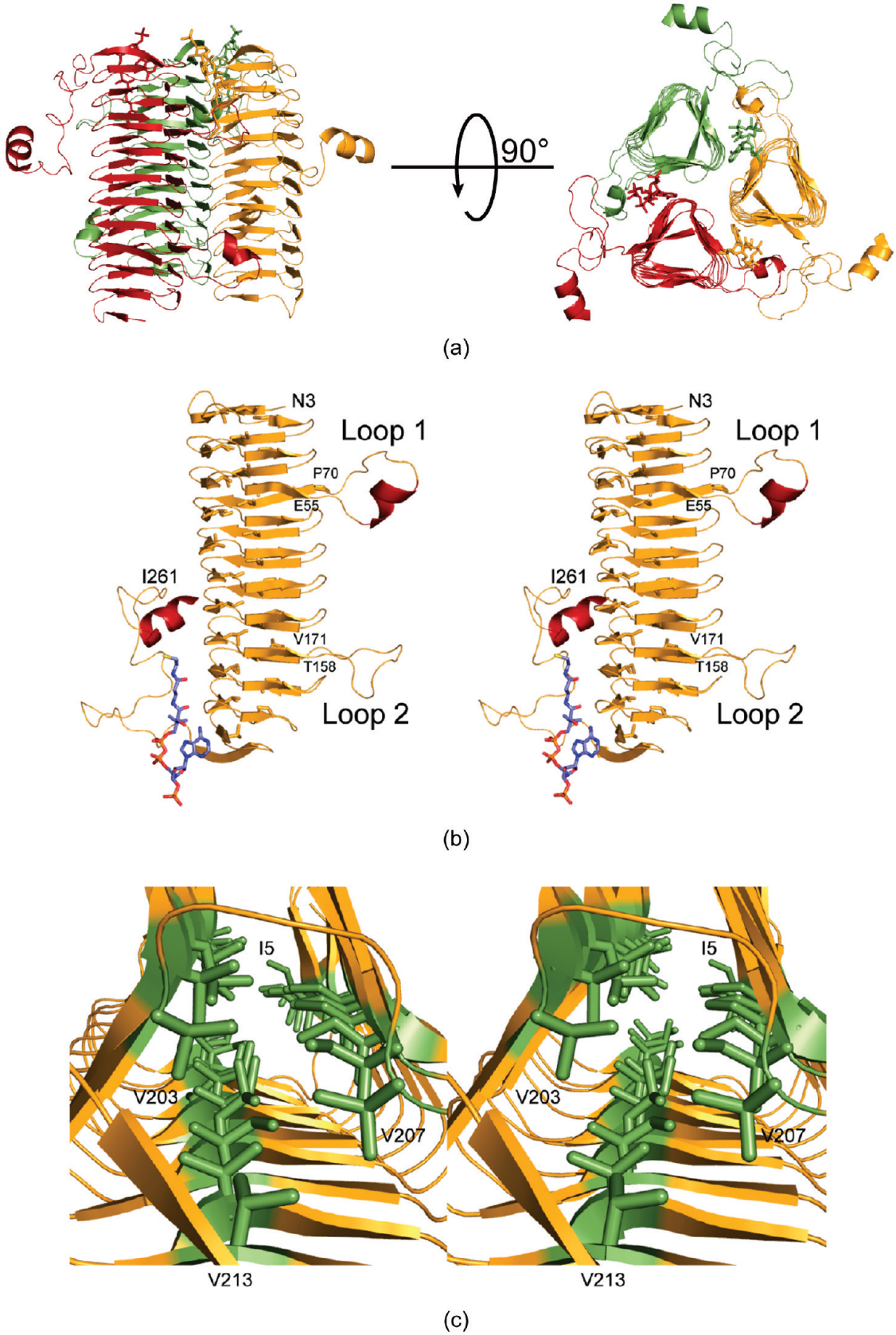


FIGURE 2: Molecular architecture of QdtC. (a) Two views of the trimeric enzyme are shown with the individual subunits color-coded in green, red, and yellow. The polypeptide chains are depicted in ribbon representations, whereas the acetyl-CoA ligands are shown as sticks. As can be seen, the three active sites of the trimer are located between subunits. (b) Stereoview of one subunit. The $\beta$-strands and $\alpha$-helices are colored orange and red, respectively. (c) Close-up view that highlights the three hydrophobic walls. These result from the hexapeptide sequence that dominates the primary structure of QdtC. All figures were prepared with PyMOL (*23*).

sulfurs, are shared between two subunits and are situated at one end of the trimer.

Shown in Figure 2b is a view of the individual subunit which is dominated by 32 $\beta$-strands that form a left-handed

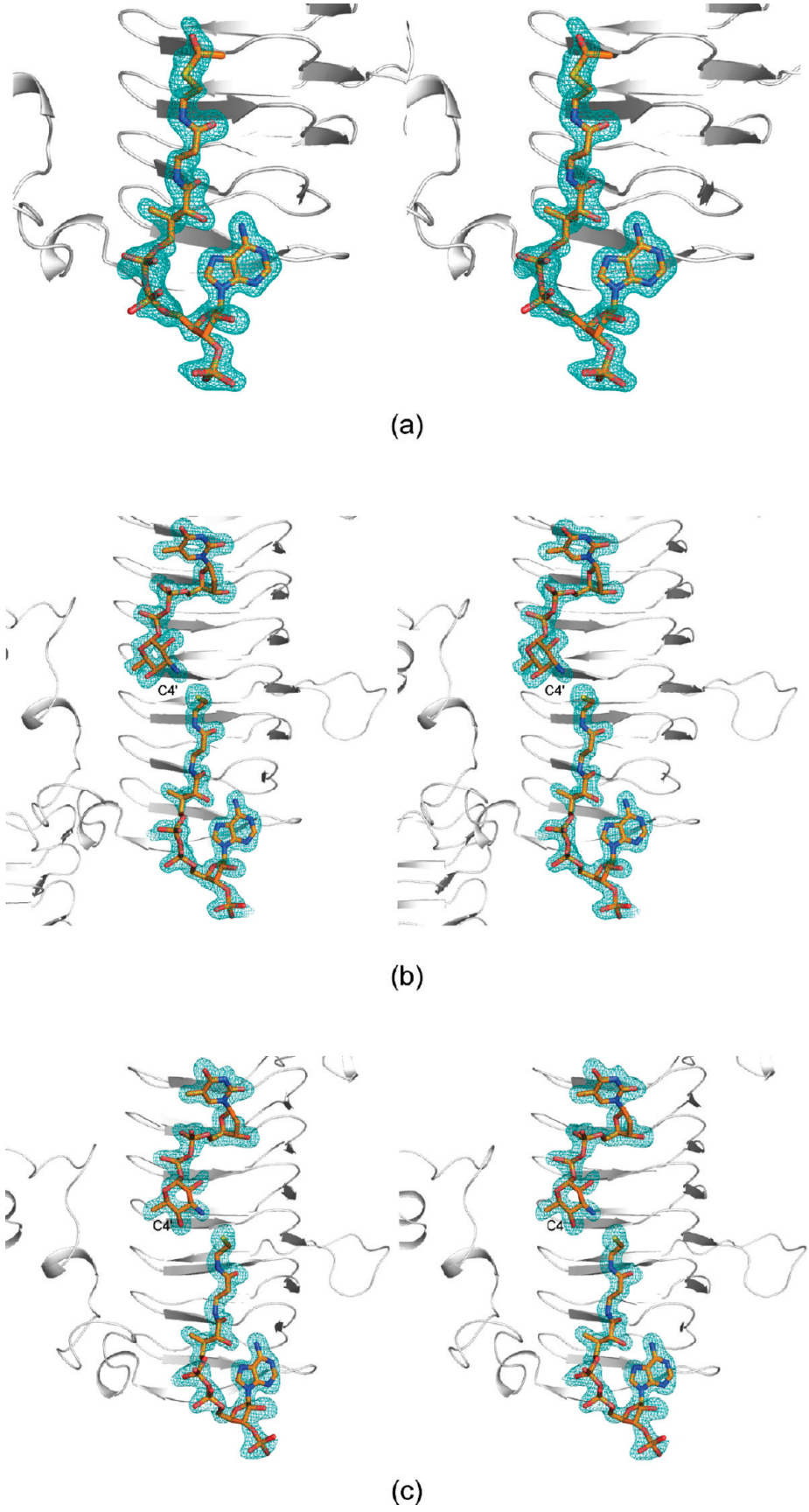


FIGURE 3: Representative electron density maps. (a) Electron density corresponding to acetyl-CoA in subunit 1 of the asymmetric unit. The map was contoured at ~3$\sigma$ and calculated with coefficients of the form $F_o - F_c$, where $F_o$ was the native structure factor amplitude and $F_c$ was the calculated structure factor amplitude. (b) Electron density corresponding to acetyl-CoA and dTDP-D-Qui*p*3N in subunit 2. The map was contoured at ~2.5$\sigma$. As can be seen, CoA rather than acetyl-CoA was observed. (c) Electron density corresponding to acetyl-CoA and dTDP-D-Fuc*p*3N in subunit 1. The map was contoured at ~3.0$\sigma$. Again, only CoA was observed.

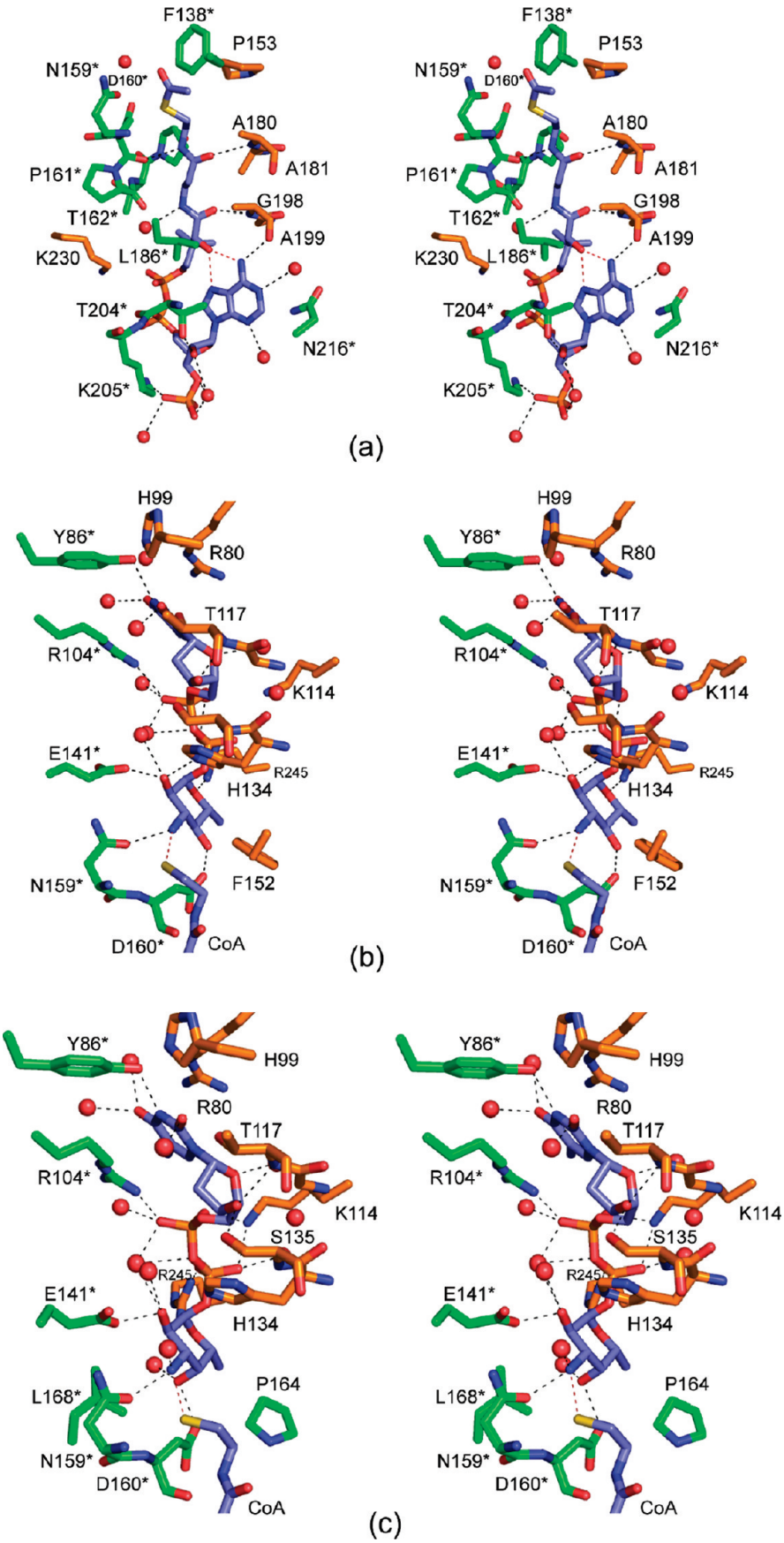


FIGURE 4: QdtC active sites with bound ligands. (a) Close-up stereoview of the QdtC active site with bound acetyl-CoA. The coenzyme is highlighted in blue bonds, whereas the residues from two of the subunits in the trimer are displayed in gold and green. For the sake of clarity, only the side chains are displayed for those residues whose backbone atoms are not involved in hydrogen bonding to the ligand. Water molecules are depicted as red spheres. Possible hydrogen bonding interactions within 3.2 Å of CoA and the protein (or solvent) are indicated by the dashed lines. (b) Close-up view of the QdtC active site with bound CoA and dTDP-D-Qui*p*3N. Given that the CoA binds in a manner nearly identical to that shown in panel a, only the immediate region surrounding the nucleotide-linked sugar is shown. (c) Close-up view of the QdtC active site with bound CoA and dTDP-D-Fuc*p*3N.

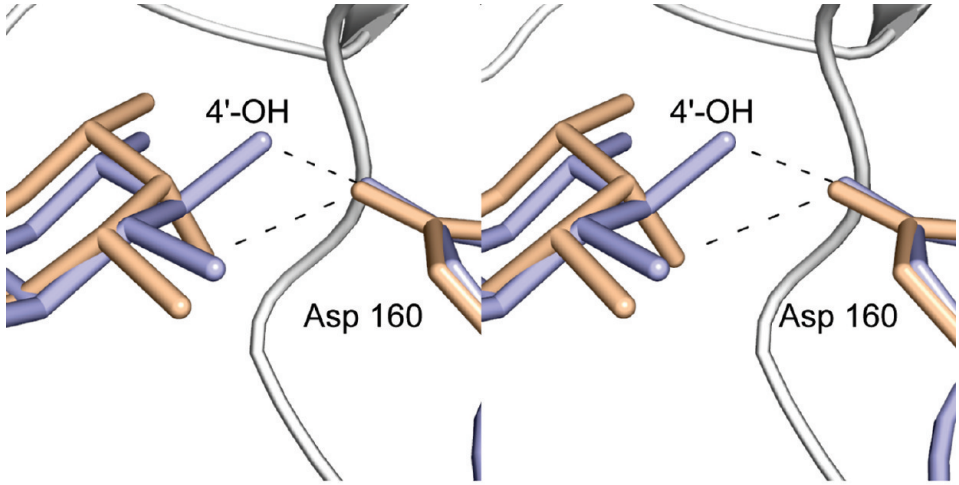


FIGURE 5: Differences in sugar binding to the QdtC active site. The dTDP-D-Qui*p*3N and dTDP-D-Fuc*p*3N ligands are colored light blue and wheat, respectively. Possible hydrogen bonds between the C-4′-hydroxyl groups of the sugars and the carboxylate of Asp 160 are indicated by the dashed lines.

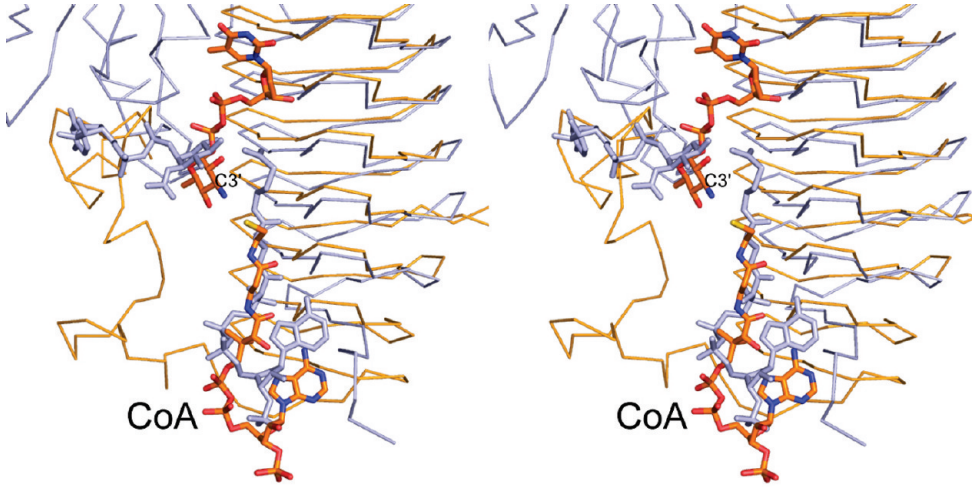


FIGURE 6: Superposition of QdtC onto PglD. The PglD structure with bound acetyl-CoA is highlighted in blue (PDB entry 3BXY). The position of the nucleotide-linked sugar, also colored blue, was obtained from the structure of the PglD determined in the presence of only the nucleotide-linked sugar (PDB entry 3BSS). The ternary complex of QdtC with bound dTDP-D-Qui*p*3N and CoA is depicted with gold bonds.

$\beta$-helix motif with 11 turns. The regularity of the $\beta$-helix is disrupted by two extended loops. The first, defined by Glu 55−Pro 70, contains an α-helix defined by Val 58−Asn 62. The second loop, delineated by Thr 158−Val 171, projects toward the active site of a symmetry-related molecule and provides a platform for accommodating the acetyl moiety of acetyl-CoA. Following the last turn of the $\beta$-helix motif, the polypeptide chain from Ile 224 to Asp 253 adopts a random coil architecture, which is capped off by the second α-helix of the subunit formed by Tyr 254−Ile 261. This α-helix extends away from the main body of the trimer (Figure 2a).

The type of left-handed $\beta$-helix motif observed in QdtC was first described in the elegant structural analysis of UDP-*N*-acetylglucosamine acyltransferase (LpxA) (*19*). Like LpxA, QdtC contains a hexapeptide repeat typically starting with an isoleucine residue, although some of the repeats begin with leucine, valine, or threonine. The first repeat begins with Ile 5 as indicated in Figure 2c. Because of this repeating motif, the interior of the $\beta$-helix is lined by three rows of mostly isoleucine residues. One row is defined by Ile 5, Ile 23, Ile 41, Ile 73, Ile 91, Ile 109, Ile 127, Ile 145, Ile 173, Ile 191, and Val 207. The second wall contains Ile 11, Ile 29, Ile 47, Ile 79, Thr 97, Ile 115, Ile 133, Leu 151, Ile 179, Val 197, and Val 213. Finally, the third row is formed by Ile 17, Ile 35, Leu 53, Ile 85, Ile 103, Ile 121, Val 139, Leu 157, Val 185, and Val 203. The regularity of the repeat breaks down at Val 203, which contains only four residues separating it from Val 207 (Figure 2c). The final hexapeptide repeat of the subunit is defined by Val 207−Val 213.

Electron density corresponding to the bound acetyl-CoA is displayed in Figure 3a. Overall, the electron density is well-defined with the exception of that for the methyl group of the acetyl moiety. The average temperature factors for the cofactors in subunits 1 and 2 of the asymmetric unit are 38.2 and 25.7 Å$^2$, respectively. As seen in Figure 3a, the acetyl-CoA adopts a curved conformation and nestles against the last four turns of the $\beta$-helix and the C-terminal loop. The ribose of the coenzyme assumes the $C_{2'}$-*endo* pucker. The phosphoryl groups of the coenzyme project outward toward the solvent, whereas the adenine ring, the pantothenate, and $\beta$-mercaptoethylamine units are quite buried within the QdtC trimer. Specifically, a total of ~350 Å$^2$ of the coenzyme's surface

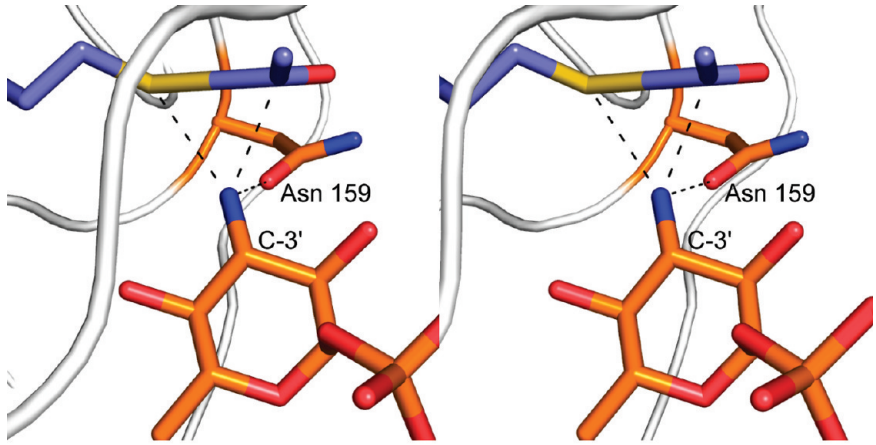


FIGURE 7: Hypothetical geometry of amino sugar attack at acetyl-CoA. According to the proposed mechanism, dTDP-D-Qui*p*3N binds to the QdtC active site in an unprotonated form. One of the hydrogens on the sugar amino group is directed at the carboxamide group of Asn 159, whereas the other is directed at the sulfur of acetyl-CoA. The nitrogen of the amino group is $sp^3$ hybridized, and the lone pair of electrons is directed toward the carbonyl group of acetyl-CoA. The model for acetyl-CoA was built on the basis of that observed in the wild-type structure.

Scheme 2

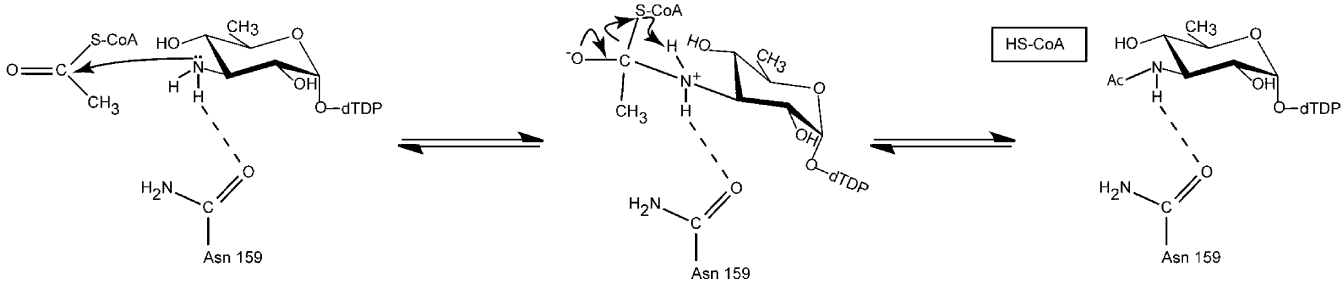


area is buried upon binding to QdtC, representing ~35% of its total surface area.

Those amino acid residues located within approximately 3.5 Å of the coenzyme are shown in Figure 4a. The adenine group of CoA is anchored to the protein via two water molecules and the carbonyl oxygen of Ala 199 from one subunit of the trimer. The side chains of Thr 204 and Lys 205 from the second subunit served to position the 2-hydroxyl and the phosphoryl group of CoA, respectively, into the QdtC active site. Additional interactions occur between the carbonyl oxygens of the pantothenate and the backbone amide nitrogens of Ala 180 and Gly 198 from one subunit. The second subunit provides a hydrogen bond between the nitrogen of the $\beta$-mercaptoethylamine unit of CoA and the backbone carbonyl of Asp 160. A total of five water molecules lies within 3.2 Å of the coenzyme. In addition to all of these interactions, two intramolecular hydrogen bonds are formed between the hydroxyl of the pantothenate moiety and N7 and the amino group of the adenine ring of CoA.

*Structure of QdtC Complexed with dTDP-D-Quip3N and CoA*. For the structural analysis of this ternary complex, the protein was first incubated with 10 mM acetyl-CoA and 40 mM dTDP-D-Qui*p*3N. The observed electron density corresponding to these ligands is displayed in Figure 3b. The nucleotide-linked sugar adopts an extended conformation and abuts four additional turns of the $\beta$-helix. It is more buried than the CoA with ~50% of its surface area covered upon protein binding.

Clearly, the electron density presented in Figure 3b demonstrates that CoA, rather than acetyl-CoA, is trapped in the active site and that the nucleotide ligand is dTDP-D-Qui*p*3N and not its acetylated version, dTDP-D-Qui*p*3NAc. Most likely during the incubation period, the protein catalyzed the acetylation reaction, thereby leading to CoA and dTDP-D-Qui*p*3NAc. Given the widely differing concentrations of acetyl-CoA and dTDP-D-Qui*p*3N used in the incubation (10 mM vs 40 mM), we speculate that all of the acetyl-CoA was hydrolyzed to CoA, which subsequently bound to the active site of QdtC in the presence of an excess of dTDP-D-Qui*p*3N. As a consequence, an abortive complex was effectively trapped within the crystalline lattice.

The binding of the dTDP-linked sugar causes little overall change in the architecture of QdtC compared to that with only bound acetyl-CoA. Indeed, the α-carbons between the two structures superimpose with a root-mean-square deviation of 0.12 Å. The manner in which CoA is accommodated in the active site of this ternary complex is similar to that observed in the acetyl-CoA−protein complex alone with some slight variations about the pyrophosphoryl groups. A close-up view of the active site surrounding the nucleotide-linked sugar is depicted in Figure 4b. As observed with acetyl-CoA, both subunits contribute to the binding of dTDP-D-Qui*p*3N. Specifically, the backbone amide nitrogen of Thr 117 from one subunit forms a hydrogen bond to the ribose hydroxyl, whereas Tyr 86 from the neighboring subunit interacts with N3 of the thymine ring. Arg 245 from one subunit and Arg 104 from the other participate in electrostatic interactions with the pyrophosphoryl groups of the substrate. The quinovose unit of the substrate, which adopts the $^4C_1$ conformation, interacts primarily with one subunit, and in particular with the second loop that interrupts the regularity of the $\beta$-helix (Figure 2b). Its 2′-hydroxyl forms a hydrogen

bond with the carboxylate of Glu 141 and the imidazole ring of His 134 (from the other subunit), whereas its C-4′-hydroxyl lies within hydrogen bonding distance of the carboxylate of Asp 160. The C-3′-amino group of the sugar is positioned within 2.9 Å of $O^{\delta 1}$ of Asn 159 and 2.9 Å of the CoA sulfhydryl group. Seven water molecules lie within 3.2 Å of the dTDP-D-Qui*p*3N molecule.

*Structure of QdtC Complexed with dTDP-D-Fucp3N and CoA.* For this structure, the enzyme was first incubated in the presence of 10 mM acetyl-CoA and 40 mM dTDP-D-Fuc*p*3N prior to crystallization. Again, only CoA and dTDP-D-Fuc*p*3N were observed in the electron density map (Figure 3c). The α-carbons for QdtC solved in the presence of either dTDP-D-Qui*p*3N or dTDP-D-Fuc*p*3N superimpose with a root-mean-square deviation of 0.14 Å, and the dTDP-sugar ligands interact with the protein in similar manners (Figure 3b,c). There is a slight movement of the hexose group in the active site such that in the case of dTDP-D-Fuc*p*3N binding, the side chain of His 134 no longer lies within 3.2 Å of the hexose 2′-hydroxyl. On the whole, however, the active site residues move very little in response to the different configuration about the C-4′-hydroxyl of dTDP-D-Fuc*p*3N. The carboxylate side chain of Asp 160 still interacts with the hexose C-4′-hydroxyl group, although the hydrogen bonding geometry is not as good as that observed for bound dTDP-D-Qui*p*3N (Figure 5). Previous activity assays have demonstrated that both dTDP-D-Qui*p*3N and dTDP-D-Fuc*p*3N are substrates for QdtC (*7*). As listed in Table 3, our kinetic data indicate an ∼50% reduction in the catalytic efficiency of QdtC with dTDP-D-Fuc*p*3N as a substrate relative to dTDP-D-Qui*p*3N.

*Enzymatic Activities of Site-Directed Mutant Proteins and Implications for a Catalytic Mechanism.* Recently, two groups reported the crystal structure of PglD, an *N*-acetyltransferase that acetylates the C-4′-amino group of UDP-2-acetamido-4-amino-2,4,6-trideoxyglucose (*20, 21*). PglD is smaller than QdtC with 203 versus 265 amino acid residues. Like QdtC, however, PglD is a trimer, and its three-dimensional architecture is dominated by a left-handed $\beta$-helix motif. The manners in which the nucleotide-linked sugars are accommodated within the active sites of PglD and QdtC are remarkably different, however, as shown in Figure 6. In PglD, His 125 has been implicated as the general base in the reaction mechanism (*20, 21*). This histidine residue is structurally conserved as His 123 in QdtC, but it is ∼8 Å from the sugar amino group. Given the observed differences in dTDP-sugar binding in PglD versus QdtC, we were concerned that perhaps our ligand bound in an artifactual manner and that His 123 might be the active site base. To test this hypothesis, two site-directed mutant proteins were constructed, H123N and H123A, and their $K_m$ and $k_{cat}$ values determined. In both cases, the mutant proteins were active with catalytic efficiencies of $2.1 \times 10^4$ and $2.0 \times 10^4$ $M^{-1}$ $s^{-1}$, respectively (Table 3). This result highlights the dangers of making biochemical assumptions based simply on amino acid sequence alignments. His 125, which is the catalytic base in PglD, aligns with His 123 of QdtC on the basis of primary sequence analyses, but clearly, the catalytic mechanisms for these two enzymes are different.

What residue then serves as the catalytic base in QdtC? There are three potential candidates, His 134, Glu 141, and Asp 160, that are located near the pyranosyl group, but they are not within hydrogen bonding distance of the sugar amino group. Again, we considered the possibility that an unusual conformation of the sugar might have been trapped in the active site and that in the Michaelis complex one of these residues resides near the sugar amino group. Thus, these residues were individually mutated to either an alanine or an asparagine in the case of His 134 and Asp 160 or a glutamine in the case of Glu 141. Again, all of these mutant proteins retained catalytic activity as indicated in Table 3. The most serious reduction in catalytic efficiency was observed for the D160A mutant protein ($2.3 \times 10$ $M^{-1}$ $s^{-1}$). In this mutant protein, the $K_m$ increased to $10.7 \pm 0.8$ mM. As a comparison, the $K_m$ for the wild-type enzyme was calculated to be $0.11 \pm 0.02$ mM. Assays in the absence of the nucleotide-linked sugar demonstrated no detectable acetyl-CoA hydrolysis for the D160A mutant protein. In addition, it should be noted that all of the mutant proteins were able to produce the acetylated sugar as demonstrated by an HPLC assay similar to that described in Materials and Methods.

Finally, to complete the story, Asn 159, which lies within hydrogen bonding distance of the sugar C-3′ amino, was changed to either an aspartate or an alanine. Again the mutant proteins were catalytically active, albeit with reduced catalytic efficiencies (Table 3). For the N159A mutant form, the $K_m$ increased to $15.4 \pm 1.5$ mM. The reduction in enzymatic activities for all of these mutant proteins most likely results from perturbations of hexose positioning in the active site and not from the loss of an enzymatic base.

In light of these observations, we propose the following mechanism for QdtC, which does not invoke a general base provided by the protein. This mechanism is outlined in Scheme 2, and a stereoview of the potential attack geometry is presented in Figure 7. Unlike that suggested for PglD, in which the nucleotide-linked sugar enters the active site in a protonated form (*21*), we suggest that QdtC binds the substrate in its unprotonated state. The carboxamide group of Asn 159 forms a hydrogen bond with the sugar C-3′-amino group, which helps to align the amino nitrogen for nucleophilic attack on the carbonyl carbon of acetyl-CoA. The other hydrogen on the amino group is directed at the sulfur of acetyl-CoA, whereas the lone pair of electrons on the nitrogen is directed at the carbonyl carbon of the cofactor. As the amino nitrogen attacks, the bond between the carbonyl carbon and the sulfur of acetyl-CoA becomes longer and eventually breaks. The sulfur of acetyl-CoA ultimately serves as the catalytic base by accepting a proton from the sugar amino group. The lack of a catalytic base in QdtC is reminiscent of the situation observed in homoserine kinase, a member of the GHMP superfamily (*22*). In this enzyme, it has been suggested that the $\gamma$-phosphoryl group of ATP, rather than an amino acid provided by the protein, ultimately serves as the base to remove the proton from the attacking hydroxyl group of homoserine. Strikingly, other members of the GHMP superfamily contain an aspartate residue in the appropriate position to function as a general base. It will be of interest to determine whether QdtC is simply an outlier like homoserine kinase or rather its catalytic mechanism is a more common feature among sugar-modifying *N*-acetyltransferases. Structural and functional studies of additional *N*-acetyltransferases are presently in progress.

## ACKNOWLEDGMENT

We thank Dr. W. W. Cleland for helpful discussions and Dr. Grover L. Waldrop for critically reading the manuscript.

## REFERENCES

1. Trefzer, A., Salas, J. A., and Bechthold, A. (1999) Genes and enzymes involved in deoxysugar biosynthesis in bacteria. *Nat. Prod. Rep. 16*, 283–299.
2. Johnson, D. A., and Liu, H.-w. (1999) *Deoxysugars: Occurrence, genetics, and mechanisms of biosynthesis*, Vol. 3, Elsevier, Amsterdam.
3. Chen, S. C., and Sorrell, T. C. (2007) Antifungal agents. *Med. J. Aust. 187*, 404–409.
4. Yoon, Y. J., Kim, E. S., Hwang, Y. S., and Choi, C. Y. (2004) Avermectin: Biochemical and molecular basis of its biosynthesis and regulation. *Appl. Microbiol. Biotechnol. 63*, 626–634.
5. Minotti, G., Menna, P., Salvatorelli, E., Cairo, G., and Gianni, L. (2004) Anthracyclines: Molecular advances and pharmacologic developments in antitumor activity and cardiotoxicity. *Pharmacol. Rev. 56*, 185–229.
6. Feng, L., Wang, W., Tao, J., Guo, H., Krause, G., Beutin, L., and Wang, L. (2004) Identification of *Escherichia coli* O114 O-antigen gene cluster and development of an O114 serogroup-specific PCR assay. *J. Clin. Microbiol. 42*, 3799–3804.
7. Pföstl, A., Zayni, S., Hofinger, A., Kosma, P., Schäffer, C., and Messner, P. (2008) Biosynthesis of dTDP-3-acetamido-3,6-dideoxy-α-D-glucose. *Biochem. J. 410*, 187–194.
8. Dong, C., Beis, K., Giraud, M. F., Blankenfeldt, W., Allard, S., Major, L. L., Kerr, I. D., Whitfield, C., and Naismith, J. H. (2003) A structural perspective on the enzymes that convert dTDP-D-glucose into dTDP-L-rhamnose. *Biochem. Soc. Trans. 31*, 532–536.
9. Novotny, R., Pfoestl, A., Messner, P., and Schaffer, C. (2004) Genetic organization of chromosomal S-layer glycan biosynthesis loci of *Bacillaceae*. *Glycoconjugate J. 20*, 435–447.
10. Davis, M. L., Thoden, J. B., and Holden, H. M. (2007) The X-ray structure of dTDP-4-keto-6-deoxy-D-glucose-3,4-ketoisomerase. *J. Biol. Chem. 282*, 19227–19236.
11. Terwilliger, T. C., and Berendzen, J. (1999) Automated MAD and MIR structure solution. *Acta Crystallogr. D55* (Part 4), 849–861.
12. Terwilliger, T. C. (2000) Maximum-likelihood density modification. *Acta Crystallogr. D56* (Part 8), 965–972.
13. Terwilliger, T. C. (2003) Automated main-chain model building by template matching and iterative fragment extension. *Acta Crystallogr. D59*, 38–44.
14. Emsley, P., and Cowtan, K. (2004) Coot: Model-building tools for molecular graphics. *Acta Crystallogr. D60*, 2126–2132.
15. Tronrud, D. E., Ten Eyck, L. F., and Matthews, B. W. (1987) An efficient general-purpose least-squares refinement program for macromolecular structures. *Acta Crystallogr. A43*, 489–501.
16. McCoy, A. J., Grosse-Kunstleve, R. W., Adams, P. D., Winn, M. D., Storoni, L. C., and Read, R. J. (2007) Phaser crystallographic software. *J. Appl. Crystallogr. 40*, 658–674.
17. Alpers, D. H., Appel, S. H., and Tomkins, G. M. (1965) A spectrophotometric assay for thiogalactoside transacetylase. *J. Biol. Chem. 240*, 10–13.
18. Magalhaes, M. L., and Blanchard, J. S. (2005) The kinetic mechanism of AAC3-IV aminoglycoside acetyltransferase from *Escherichia coli*. *Biochemistry 44*, 16275–16283.
19. Raetz, C. R., and Roderick, S. L. (1995) A left-handed parallel $\beta$ helix in the structure of UDP-*N*-acetylglucosamine acyltransferase. *Science 270*, 997–1000.
20. Rangarajan, E. S., Ruane, K. M., Sulea, T., Watson, D. C., Proteau, A., Leclerc, S., Cygler, M., Matte, A., and Young, N. M. (2008) Structure and active site residues of PglD, an *N*-acetyltransferase from the bacillosamine synthetic pathway required for *N*-glycan synthesis in *Campylobacter jejuni*. *Biochemistry 47*, 1827–1836.
21. Olivier, N. B., and Imperiali, B. (2008) Crystal structure and catalytic mechanism of PglD from *Campylobacter jejuni*. *J. Biol. Chem. 283*, 27937–27946.
22. Zhou, T., Daugherty, M., Grishin, N. V., Osterman, A. L., and Zhang, H. (2000) Structure and mechanism of homoserine kinase: Prototype for the GHMP kinase superfamily. *Struct. Folding Des. 8*, 1247–1257.
23. DeLano, W. L. (2002) *The PyMOL Molecular Graphics System*, DeLano Scientific, San Carlos, CA.

BI802313N